Journal of Computational Neuroscience 13, 93–109, 2002

States of High Conductance in a Large-Scale Model of the Visual Cortex

MICHAEL SHELLEY, DAVID McLAUGHLIN, ROBERT SHAPLEY AND JACOB WIELAARD
Center for Neural Science & Courant Institute of Mathematical Sciences, New York University, NY 10012, USA
shelley@cims.nyu.edu

Received November 19, 2001; Revised April 22, 2002; Accepted May 10, 2002

Action Editor: Xiao-Jing Wang

Abstract. This paper reports on the consequences of large, activity dependent, synaptic conductances for neurons in a large-scale neuronal network model of the input layer $4C\alpha$ of the Macaque primary visual cortex (Area V1). This high conductance state accounts for experimental observations about orientation selectivity, dynamics, and response magnitude (D. McLaughlin et al. (2000) *Proc. Natl. Acad. Sci. USA* 97: 8087–8092), and the linear dependence of Simple cells on visual stimuli (J. Wielaard et al. (2001) *J. Neuroscience* 21: 5203–5211). The source of large conductances in the model can be traced to inhibitory corticocortical synapses, and the model's predictions of large conductance changes are consistent with recent intracellular measurements (L. Borg-Graham et al. (1998) *Nature* 393: 369–373; J. Hirsch et al. (1998) *J. Neuroscience* 15: 9517–9528; J.S. Anderson et al. (2000) *J. Neurophysiol.* 84: 909–926). During visual stimulation, these conductances are large enough that their associated time-scales become the shortest in the model cortex, even below that of synaptic interactions. One consequence of this activity driven separation of time-scales is that a neuron responds very quickly to temporal changes in its synaptic drive, with its intracellular membrane potential tracking closely an *effective reversal potential* composed of the instantaneous synaptic inputs. From the effective potential and large synaptic conductance, the spiking activity of a cell can be expressed in an interesting and simplified manner, with the result suggesting how accurate and smoothly graded responses are achieved in the model network. Further, since neurons in this high-conductance state respond quickly, they are also good candidates as coincidence detectors and burst transmitters.

Keywords: primary visual cortex, neuronal network model, time-scales, orientation hypercolumn, synaptic conductances, inhibitory conductances

In recent work we have developed a large-scale computational model of an input layer of the Macaque Primary Visual Cortex (V1), for the purpose of studying cortical response. The model describes a small patch (1 mm^2) of the cortical layer $4C\alpha$, and contains four orientation hypercolumns with pinwheel centers. This model captures qualitatively the observed selectivity, diversity, and dynamics of orientation tuning of neurons in $4C\alpha$ when under visual stimulation by either drifting or randomly flashed gratings (McLaughlin et al., 2000). And remarkably for a nonlinear network, it captures also the linear dependence of Simple cells upon visual stimuli (Wielaard et al., 2001).

Our many numerical experiments indicate that, as the model cortex acts like the biological cortex, it operates in restricted regions of its parameter and phase space—regions of very large membrane conductances which result from network activity (and not from the properties of individual cells). These large conductances have cortico-cortical components which are dominated by inhibition, which seems necessary if the model is to produce background firing statistics that are consistent

with experimental measurement (Mechler, 1997) while also accounting for the observed properties of orientation selectivity and linearity of Simple cells.

In what way do large conductances influence cortical response? Together, the total membrane conductance g_T and the capacitance C set the membrane time-scale $\tau_g = C/g_T$. Among other time-scales of a cortical cell—a leakage time, the period of a visual stimulus, the time-scale of a single EPSP or IPSP ("synaptic time-scales")—τ_g has the unique property that it reflects the level of network activity. That is, increases in a network's synaptic activity give increases in cellular membrane conductances, which shorten the time-scale of response, τ_g, of individual neurons. But by how much? We find that under high contrast visual stimulation these large membrane conductances cause τ_g to emerge as the *shortest time-scale*, shorter than the other time-scales in the model cortex, and in particular shorter than those governing temporal fluctuations in the synaptic conductances. This is what we mean by "large conductance". A neuron in this network acts not as a leaky integrator of its inputs, but instead as a near-instantaneous function of its cortical and thalamic input conductances. The existence of this high conductance state allows us to analyze the intracellular membrane potential and spiking activity of cortical neurons in a new way, using the asymptotic analysis offered in *Results*. We find too that the close tracking of synaptic fluctuations afforded by the presence of high conductance yields an average firing rate that is a smoothly graded computation of the ratio of excitatory to inhibitory inputs to a cell.

While we found these short, activity-dependent membrane time-scales in our investigations of the visual cortex, this scale separation is likely to be characteristic of neurons throughout the cerebral cortex. Thus, the analysis offered here should be of general utility for understanding cortical behavior.

Methods

The Computational Model

The model (described in detail in McLaughlin et al. (2000) and Wielaard et al. (2001)) is of a small local patch (1 mm^2) of layer 4$C\alpha$—consisting of a two dimensional lattice of 128^2 coupled, integrate-and-fire (I&F) neurons, of which 75% are excitatory and 25% are inhibitory. The membrane potentials of excitatory (inhibitory) neurons are denoted by $v_E^j(v_I^j)$, which satisfy

$$\frac{dv_P^j}{dt} = -g_L v_P^j - g_{PE}^j(t)\big[v_P^j - V_E\big] - g_{PI}^j(t)\big[v_P^j - V_I\big], \tag{1}$$

where $P = E, I$ and the superscript $j = (j_1, j_2)$ indexes the spatial location of the neuron within the cortical layer. We specified the cellular biophysical parameters, using commonly accepted values (Koch, 1999): the capacitance $C = 10^{-6}$ Fcm^{-2}, the leakage conductance $g_L = 50 \times 10^{-6}\ \Omega^{-1}\,\mathrm{cm}^{-2}$, the leakage reversal potential $V_R = -70$ mV, the excitatory reversal potential $V_E = 0$ mV, the inhibitory reversal potential $V_I = -80$ mV, the spiking threshold $\bar{v} = -55$ mV, and the reset potential set at the leakage reversal potential, -70 mV.

We have normalized the potentials by the transformation $v \to (v - V_R)/(\bar{v} - V_R)$, making them dimensionless quantities. This normalization sets the spiking threshold $\bar{v}$ to unity, the reset potential to zero, $V_E = 14/3$, and $V_I = -2/3$. Within this normalization, the potentials range over $-2/3 \le v_E^j, v_I^j \le 1$. To convert back to dimensional quantities, insert the dimensionless v into the formula

$$v_{\mathrm{mV}} = (\bar{v} - V_R)v + V_R.$$

The capacitance C does not appear in Eq. (1) as all conductances have been defined as rates, with units of s^{-1}, by dividing through by C. This convention emphasizes the time-scales which the conductances represent. For example, the leakage conductance $g_L = 50\ \mathrm{s}^{-1}$ produces a leakage time-scale $\tau_L = g_L^{-1} = 50^{-1}\,\mathrm{s} = 20$ ms. True conductances are obtained by multiplying by the capacitance $C = 10^{-6}\,\mathrm{F\,cm}^{-2}$.

Conductances

The time-dependent conductances arise from the input forcing (through the LGN) and from noise to the layer, as well as from the cortical network activity of the excitatory and inhibitory populations. They have the form:

$$g_{EE}^j(t) = F_{EE}(t) + S_{EE}\sum_k a_{j-k}\sum_l G_E\big(t - t_l^k\big),$$
$$g_{EI}^j(t) = f_{EI}^0(t) + S_{EI}\sum_k b_{j-k}\sum_l G_I\big(t - T_l^k\big),$$

with similar expressions for g^j_{IE} and g^j_{II}, and where $F_{PE}(t) = g^j_{lgn}(t) + f^0_{PE}(t)$, $P = E, I$. Here $t^k_l(T^k_l)$ denotes the time of the lth spike of the kth excitatory (inhibitory) neuron. Note that $g_{EE}(g_{EI})$ is the conductance driven by excitatory (inhibitory) network activity, and that the first "E" labels the postsynaptic target as an excitatory cell.

The conductances $f^0_{PP'}(t)$ are stochastic, and represent activity from other areas of the brain, say inputs to layer $4C\alpha$ from layer 6. These conductances have means and standard deviations given by $f^0_{EE} = f^0_{IE} = 6 \pm 6\ \mathrm{s}^{-1}$, $f^0_{EI} = f^0_{II} = 85 \pm 35\ \mathrm{s}^{-1}$, and they have an exponentially decaying autocorrelation function with time constant 4 ms. The constant background g_0 of the LGN drive g_{lgn} is taken as $35\ \mathrm{s}^{-1}$. The kernels $(a, b, \ldots)$ represent the spatial coupling between neurons, and reflect our understanding of cortical anatomy (Lund, 1987; Lund and Yoshioka, 1991; Callaway and Wiser, 1996; Wiser and Callaway, 1996; Lund and Wu, 1997; Callaway, 1998). Only local cortical interactions (i.e. within a hypercolumn) are included in the model, and these are assumed to be isotropic, with Gaussian profiles for the kernels $(a, b, \ldots)$ (McLaughlin et al., 2000). The spatial length-scale of excitation exceeds that of inhibition, and we estimate excitatory radii of order 200 μm and inhibitory radii of order 100 μm.

The cortical temporal kernels $G_\sigma(t)$ model the time-course of synaptic conductance changes in response to arriving spikes from the other neurons. They are of the form

$$G_\sigma = c_\sigma \frac{t^5}{\tau^6_\sigma} \exp(-t/\tau_\sigma) H(t), \quad \sigma = E, I,$$

where $H(t)$ is the unit step function. The time constants are chosen to give a time-to-peak of 3 ms for excitation (with that time-course ending by approximately 8 ms) and time-to-peak of 5 ms for inhibition, which are consistent with experimental observations (Koch, 1999; Azouz et al., 1997; and A. Reyes, private communication). In addition, based on recent experimental findings, we add a second, longer time-course of inhibition (Gibson et al., 1999) ($\sim$30 ms in duration).

As should be clear from the above, it is difficult to assign a single time-scale to represent synaptic fluctuations. The excitatory time-course suggests some value between 3 and 8 ms, while the time-scales for inhibition are longer. As a reference scale we choose $\tau_{syn} = 4$ ms, and capture the faster time-scales of excitatory synaptic fluctuations (and hence, also those of inhibition). We have also chosen the noise to fluctuate on that time-scale, as the noise represents synaptic events.

The computational model's behavior depends on the choice of the cortico-cortical synaptic coupling coefficients: S_{EE}, S_{EI}, S_{IE}, S_{II}. All cortical kernels have been normalized to unit area. Hence, the coupling coefficients represent the strength of interaction, and are treated as adjustable parameters in the model. In the numerical experiments reported here, the strength matrix $(S_{EE}, S_{EI}, S_{IE}, S_{II})$ was set to be (0.8, 9.4, 1.5, 9.4). This matrix means that excitatory neurons excite inhibitory neurons almost twice as much as they excite other excitatory neurons, but that inhibitory neurons inhibit excitatory neurons and other inhibitory neurons with equal strength. Also, inhibitory neurons have much stronger coupling to all other cortical neurons than do excitatory neurons. We explored many strength matrices in many numerical experiments. If the cortico-cortical excitation was too strong, oscillations resulted. If the cortico-cortical inhibition was too weak, the cells' responses were nonlinear and not selective enough. If inhibition was too strong, the network's response became too small. The matrix given here generated Simple cells that had the orientation selectivity, and the magnitude and dynamics of response, seen in physiological experiments (McLaughlin et al., 2000).

Visual Stimuli

For *drifting gratings*, the visual stimulus on the "screen" has intensity pattern $I = I(x, t; \theta, \phi, k, \omega, I_0, \epsilon)$ given by

$$I = I_0[1 + \epsilon \cos[\vec{k} \cdot \vec{x} - \omega t + \phi]]. \qquad (2)$$

where $\vec{k} = k(\cos\theta, \sin\theta)$. Here $\theta \in [-\pi, \pi)$ denotes the orientation of the sinusoidal pattern on the screen, $\phi \in [0, 2\pi)$ denotes its phase, $\omega \geq 0$ its frequency, I_0 its intensity, and ϵ its "contrast". Drifting gratings have been used in many neurophysiological experiments to characterize spatial properties of visual neurons in macaque V1 (De Valois et al., 1982).

For *randomly flashed patterns*, Eq. (2) is still used, but as a random sequence of standing gratings with $\omega = 0$ and $\theta \in [0, \pi)$. After switching on the grating at $t = 0$, the screen is refreshed each τ_R (17 msecs), and a new pattern is chosen randomly (and independently) from a collection of patterns which consists of $N + 1$ values of the orientation $\{\theta = k\pi/N, k = 0, 2, \ldots, N\}$ and M values of the phase

$\{\phi = k2\pi/M, k = 1, 2, \ldots, M\}$. Each orientation is equally likely, as is each choice of phase. For the random pattern $\theta = \pi, \epsilon$ is set at 0; hence, this pattern represents a "blank" screen. Randomly flashed gratings have been used to study the dynamics of orientation selectivity in the cortex (Ringach et al., 1997).

LGN Response to Visual Stimuli

The total input into the jth cortical neuron arrives from $N(=17)$ LGN cells:

$$g^j_{lgn}(t) = \sum_{i=1}^{N} \left\{ g^j_0 + \int_0^t ds \int d^2x G_{lgn}(t-s) \times A\left(\vec{x}^j_i - \vec{x}\right) I(\vec{x}, s) \right\}^+. \quad (3)$$

Here $\{R\}^+ = R$ if $R > 0; \{R\}^+ = 0$ if $R \leq 0; g^j_0$ represents the maintained (background) activity of the LGN neurons feeding into the jth cortical neuron, in the absence of visual stimulation. The temporal kernel $G_{lgn}(t)$ and spatial kernel $A(\vec{x})$ of an LGN cell are chosen to agree with experimental measurements (Benardete and Kaplan, 1999; Shapley and Reid, unpublished observations). (See McLaughlin et al., 2000; Wielaard et al., 2001).)

Results

Again, throughout this article we will use conductances normalized as rates ($\sec^{-1}$) in order to emphasize the time-scales which they represent. For our analysis, we turn to Eq. (1) which governs a model cell's response to conductance changes, written in the form:

$$\frac{dv}{dt} = -g_T(t)v(t) + I_D(t) = -g_T(t)[v(t) - V_s(t)]. \quad (4)$$

Here, g_T is the total conductance of the model neuron, given by

$$g_T(t) \equiv g_L + g_E(t) + g_I(t), \quad (5)$$

where g_E and g_I are the excitatory and inhibitory conductances at time t. The conductance g_T reflects several time-scales inherent in the operation of the computational cortex under visual stimulation: (i) the time-scale of the visual stimulus, $\tau_{lgn} = O(10$–10^2 ms); (ii) the base cellular time-scale of leakage, $\tau_L = 20$ ms; (iii) the synaptically mediated cortico-cortical interactions which govern the fluctuations in g_E and g_I, $\tau_{syn} = 4$ ms; and (iv) the conductance time-scale, $\tau_g = [g_T^{-1}]$ (where $[\cdot]$ denotes some characteristic size). One important distinction being made here is between the temporal scales of fluctuation in g_T (i.e. points (i) and (iii)), and the time-scale implicit in the *magnitude* of g_T (point (iv)).

The quantities I_D and V_S are defined by

$$I_D(t) = I_D[g_E(t), g_I(t)] \equiv g_E(t)V_E - g_I(t)|V_I|, \quad (6)$$

$$V_S(t) = V_S[g_E(t), g_I(t)] \equiv I_D(t)/g_T(t). \quad (7)$$

We call I_D the *difference current*, as it is a difference of currents arising from excitation and inhibition, and V_S is called the *effective reversal potential* (see Wielaard et al. (2001) for a discussion of the role of these quantities in understanding the appearance of Simple cells in our cortical model). Note that (i) $g_T(t)$ and $V_S(t)$ are explicit functions of the instantaneous synaptic input conductances $g_E(t)$ & $g_I(t)$, and (ii) a *necessary condition* for $v(t)$ to cross the spiking threshold is that $V_S > 1$, i.e., V_S itself is above threshold. (This follows directly from Eq. (4), and the requirement that $v(t_s) = 1$ while $dv(t)/dt|_{t=t_s} > 1$ at a spike time t_s.)

First, we show that our detailed and large-scale cortical network model (consisting of many I&F point-neurons) develops large conductances when under visual stimulation, and that these conductance changes have magnitudes that are consistent with recent experimental and theoretical observations. In our model network, such large conductances mean that the membrane time-scale τ_g emerges as the shortest time-scale of the system. To make theoretical progress, we will assume that τ_g is *well-separated* from any other time-scale, and show through an asymptotic analysis that the dynamics of such a model neuron is greatly simplified in its response to synaptic inputs. This simplification is in the form of I/O relations that express a cell's intracellular potential and firing rate directly in terms of its instantaneous synaptic conductances. Next, we show from our large-scale network simulations that neuronal responses are predicted with surprising accuracy by these I/O relations. In previous work (McLaughlin et al., 2000) we emphasized within our cortical model the differences in orientation selectivity of neurons which are near and far from orientation pinwheel centers. At the end of *Results*, we describe also near/far

differences for the total conductance, in both its mean and fluctuations, and show "conductance maps on the cortex".

The Emergence of Different Time-Scales in the Model Cortex

Figures 1a and b shows the time-dependent total conductances of a typical, orientation selective excitatory neuron within our large-scale cortical model. This neuron is located far from an orientation pinwheel center, and is stimulated at its preferred, and orthogonal-to-preferred, orientations by an 8 Hz drifting grating (also set at optimal spatial and temporal frequency and high contrast). The visual stimulation is switched on at $t = 0.5$ sec.

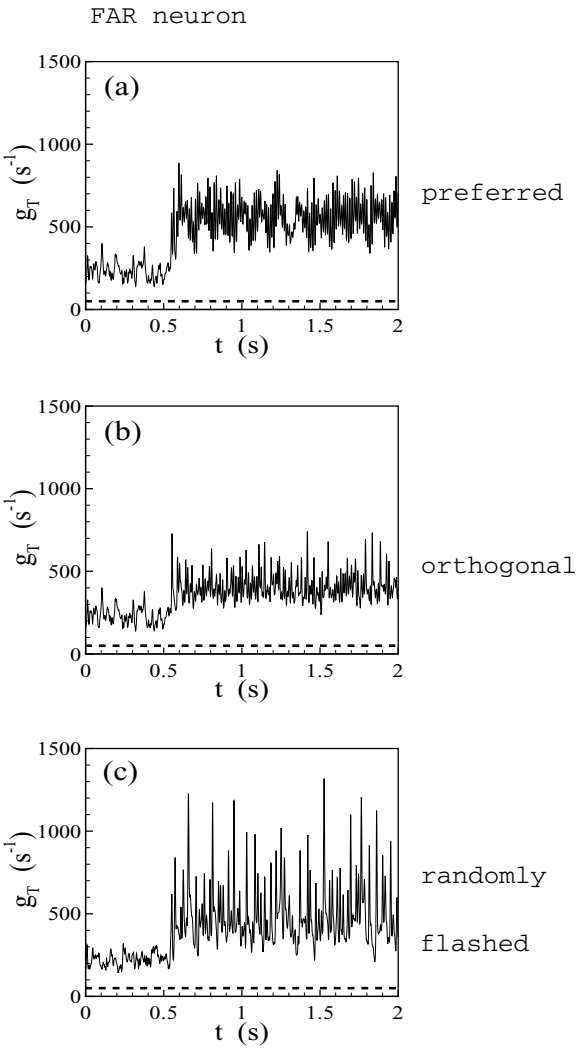

Figure 1. Total conductance $g_T(t)$ vs t for a typical orientation selective excitatory neuron, located far from pinwheel centers. The stimuli are switched on at $t = 0.5$ sec. Figures a and b are for a drifting grating stimulus at (a) preferred and (b) orthogonal-to-preferred orientation (drifting at 8 Hz, with optimal spatial and temporal frequency and 100% contrast). The response to randomly flashed gratings is shown in (c). The dashed line marks the level of the base leakage conductance (50 s^{-1}).

First note that even when unstimulated ($t < 0.5$ s), the total conductance is always much higher than the leakage conductance of individual cells: In unstimulated background, $g_T = 230 \pm 40$ s^{-1} (mean $\pm$ standard deviation) versus $g_L = 50$ s^{-1}, or a time-scale of $\tau_g \simeq 4$ ms versus $\tau_L = 20$ ms. In this case, τ_g and τ_{syn} are roughly in balance, and are the shortest time-scales. However, with the onset of visual stimulation at the preferred orientation, Fig. 1a shows that the total conductance of the model neuron undergoes a two-fold increase, producing $g_T = 550 \pm 100$ s^{-1}, with the associated conductance time-scale decreasing to $\tau_g \simeq 2$ ms. When stimulated at the orthogonal-to-preferred orientation, $g_T = 400 \pm 80$ s^{-1} (Fig. 1b), which while considerably less than at preferred, is still nearly twice its unstimulated value.

Figure 1c also shows the total conductance, but now for randomly flashed grating stimuli (switched on at $t = 0.5$ sec). As described in *Methods*, these stimuli are chosen randomly from a collection of high contrast standing gratings, with the screen refreshed every 17 msec. Again, there is a large conductance increase with the onset of visual stimulation: $g_T = 480 \pm 175$ s^{-1}.

In all cases—drifting grating stimuli at either preferred or orthogonal-to-preferred orientation, or randomly flashed gratings—the large conductances induced by visual stimulation cause the membrane time-scale τ_g to drop below τ_{syn}, the synaptic time-scale, and hence become the shortest time-scale in the system.

Comparisons with Experiment

Our model requires strong inhibition to operate realistically when compared with experimental observations. The network's consequent cortical activity produces conductance values that are very large: Background activity provides a factor of 4–5 over cellular leakage values (as suggested by Bernander et al. (1991)), and high contrast visual stimulation provides an additional factor of 2.

Accurate values of in vivo conductances are extremely difficult to measure. Hence, recent experiments have focused on the demonstration of the presence of large conductance *changes* under visual stimulation. In the cat visual cortex, Borg-Graham et al. (1998) have studied the intracellular responses of Simple cells to flashed bars. Using in vivo whole-cell voltage clamping, they measured the dynamics of conductance during visual stimulation and found two- to three-fold conductance increases over unstimulated background. They associate these large conductances with the activation of strong cortico-cortical inhibition. Hirsch et al. (1998) have also performed in vivo whole-cell patch recordings of Simple cells in cat cortex. Their results likewise suggest strong cortico-cortical inhibition arising in response to visually-driven, excitatory geniculate input, with this inhibition driving large increases in total membrane conductance. Most recently, Anderson et al. (2000) confirmed the presence of these large conductance changes induced by high contrast visual stimulation for cat. Our numerical observations (Tables 1 and 2, and Figs. 1, 2, 4, 7, and 8) of conductance changes of more than 200%, caused by visual stimulation, are qualitatively consistent with these intracellular measurements.

Time-Scales, Asymptotic Representations, and Neuronal Response within a High Conductance State

In our model cortex, large conductances induced by visual stimulation cause τ_g to be the shortest time-scale present. If g_T is sufficiently high that τ_g is well separated from all other time-scales in the cortex, we now show that one can use asymptotic analysis to derive useful (I/O) relations that express the membrane potential and the interspike times of a cell directly in terms of its synaptic conductances. We will return later to answer the question whether the conductances observed in the model are actually high enough to achieve the consequences of time-scale separation used in our analysis.

It is clear intuitively from the structure of Eq. (4) that if g_T is sufficiently large, a neuron in this high conductance state will possess two characteristic response properties:

1. When *subthreshold*, the membrane potential is well approximated by the effective reversal potential $V_S(t)$. As this reversal potential is also an explicit function of the instantaneous input conductances to the cell, we write
$$v(t) \simeq V_S(t) = V_S[g_E(t), g_I(t)].$$
2. When forced away from $V_S(t)$ (as when $v(t)$ spikes), the membrane potential returns quickly to being very close to $V_S(t)$.

We now define precisely the notion of time-scale separation, and use it to develop I/O relationships through asymptotic arguments. Let τ_g be an average value of g_T^{-1}, and let τ_{syn} be a time-scale governing the fluctuations of synaptic conductances. We then express V_S and g_T as $V_S(t/\tau_{syn})$ and $g_T(t/\tau_{syn})$, both are defined in terms of these conductances. Then rescaling time and total conductances as $\tilde{t} \equiv t/\tau_{syn}$ and $\tilde{g}_T \equiv g_T\tau_g$, and defining the ratio of time-scales, $\epsilon \equiv \tau_g/\tau_{syn}$, Eq. (4) becomes:

$$\epsilon\frac{dv}{d\tilde{t}} = -\tilde{g}_T(\tilde{t})(v - V_S(\tilde{t})). \tag{8}$$

If $\epsilon = O(1)$ or larger, then the cell smoothes the synaptic input over an $O(1)$ (synaptic) time-scale. That is, the cell acts as an integrator. If instead $\epsilon \ll 1$, the cell will respond almost instantaneously to its synaptic input.

(For clarity in discussing the asymptotic analysis, we will continue use of the notation $\tilde{t}$, $\tilde{g}$, ... to emphasize when time is being scaled by τ_{syn}.)

By introducing an "intrinsic" and dimensionless time $u \equiv \int_0^{\tilde{t}} g(\tilde{t}')\,d\tilde{t}'$, and expressing v and V_S in terms of it, Eq. (8) takes the form

$$\epsilon\frac{dv}{du} = -(v - V_S(u)).$$

Let $v(u_{in}) = v_{in}$ be the voltage at the initial time u_{in}. The equation can be immediately integrated to yield

$$v(u) = v_{in}\exp\left\{-\frac{u-u_{in}}{\epsilon}\right\} + \frac{1}{\epsilon}\int_{u_{in}}^{u}\exp\left\{-\frac{u-u'}{\epsilon}\right\}V_S(u')\,du'.$$

This expression can then be successively integrated by parts to develop the following asymptotic expansion in small ϵ:

$$v(u) = \left[V_S(u) - \epsilon\frac{dV_S}{du}(u) + \epsilon^2\frac{d^2V_S}{du^2}(u) - \cdots\right] + \exp\left\{-\frac{u-u_{in}}{\epsilon}\right\}\left[v_{in} - V_S(u_{in}) + \epsilon\frac{dV_S}{du}(u_{in}) - \epsilon^2\frac{d^2V_S}{du^2}(u_{in}) + \cdots\right]. \tag{9}$$

Note that the first term (in brackets) is independent of initial data, and is V_S to leading order, while the second term shows the rapid loss of dependence of the solution upon its initial data. Indeed, Formula (9) shows two characteristic features of neurons within a high conductance state:

(i) When *subthreshold* and $u - u_{in} \gg \epsilon$, Formula (9) shows that the membrane potential is indeed slaved to the effective reversal potential V_S:

$$v(\tilde{t}) = V_S(\tilde{t}) - \frac{\epsilon}{\tilde{g}_T(\tilde{t})}\frac{dV_S}{d\tilde{t}} + O(\epsilon^2), \qquad (10)$$

where V_S is, again, defined in terms of the instantaneous synaptic conductances by Eq. (7). Moreover, this analysis also shows that membrane potential lags in time behind V_S, as the expansion in Eq. (10) can be reordered and expressed as

$$v(\tilde{t}) = V_S\left(\tilde{t} - \frac{\epsilon}{\tilde{g}_T(\tilde{t})}\right) + O(\epsilon^2), \qquad (11)$$

That is, the first order correction can be reinterpreted as a backwards time shift of V_S, with the time shift given by the scaled total conductance itself, and with amplitude corrections to v only appearing only at next order, $O(\epsilon^2)$.

(ii) The second feature described by Eq. (9) is the very rapid response of neurons in the high conductance regime: After $v(\tilde{t})$ is forced away from $V_S(\tilde{t})$ (as when the neuron spikes at $\tilde{t}_k$), the membrane potential very rapidly attempts to return to the neighborhood of $V_S(\tilde{t})$:

$$v(\tilde{t}) - V_S(\tilde{t}) = O(\epsilon) + O(e^{-u/\epsilon}), \quad \text{where}$$
$$u \equiv \int_{\tilde{t}_k}^{\tilde{t}} \tilde{g}(\tilde{t}')\, d\tilde{t}', \quad \tilde{t} > \tilde{t}_k. \qquad (12)$$

That is, within a basically $O(\epsilon)$ time from v being displaced from V_S, say at a spike time $\tilde{t}_k$, v returns to its neighborhood. If V_S happens to be above threshold, this rapid return will likely lead to another spike.

Slaving in the Model Cortex

We showed that when under high contrast visual stimulation, the membrane time-scale τ_g emerged in our computational cortex as the shortest time-scale. We show now that neurons in this computational cortex are also described with surprising fidelity by our asymptotic analysis, even though τ_g lies below the synaptic time-scale τ_{syn} by only a factor of two. This claim is well illustrated by Fig. 2a: It shows the membrane potential $v(t)$ (green curve) for the excitatory neuron of Fig. 1c, where the model cortex is being driven by the randomly flashed grating stimulus, and its effective reversal potential $V_S(t)$ (red curve), calculated from Eq. (7) as the ratio I_D/g_T (time is again dimensional). The total conductance g_T is also shown (dashed blue, in units of sec^{-1}).

While V_S is subthreshold, $v(t)$ tracks $V_S(t)$ closely and the two are nearly identical. First, recall that Eq. (11) predicts that $v(t)$ is nearly a leftward shifted copy of V_S, with the size of the shift inversely proportional to g_T. Figure 2a and c confirms this feature of the potential. Note too that the rises in V_S above threshold, and thus the onset of spiking activity, are associated with dips in the total conductance. These decreases in g_T are tied to decreases in the inhibitory conductance, and thus the spiking activity shown here arises from a release from inhibition.

There is some experimental indication that neurons in the cortex in vivo actually respond in the slaved fashion of the neurons in the model. Specifically, Fig. 1 of Borg-Graham et al. (1998) can be interpreted as showing that, immediately after the stimulus is switched on, the voltage is "slaved" to an effective reversal potential, during which time the conductance is very large.

For comparison, Fig. 2b shows $v(t)$ and $V_S(t)$ for an unstimulated neuron (i.e., $t < 0.5$ s). Again the scale of g_T is set by leakage, the stochastic conductances, and a now *weaker* network activity. The membrane time-scale τ_g is now larger than that under stimulation, and comparable to that of synaptically mediated fluctuations in V_S. Nonetheless, Fig. 2b shows that $v(t)$ still tracks $V_S(t)$, though more loosely since ϵ is larger than under stimulation. Figure 2c–f shows the dynamics over a smaller (50 ms) time interval. In Fig. 2c and d, the neuron is subthreshold, with and without stimulation; while in Fig. 2e and f, the neuron is spiking, with and without stimulation. A significant difference between the stimulated and unstimulated cases, as seen in Fig. 2, is the recovery time after spike reset—which sets a (local in time) frequency for spiking. During stimulation by randomly flashed gratings, this recovery time is one-half of its background value, which is in register with the changes in the conductance time-scales: $\tau_g^{back} \simeq 4$ ms versus $\tau_g^{stim} \simeq 2$ ms.

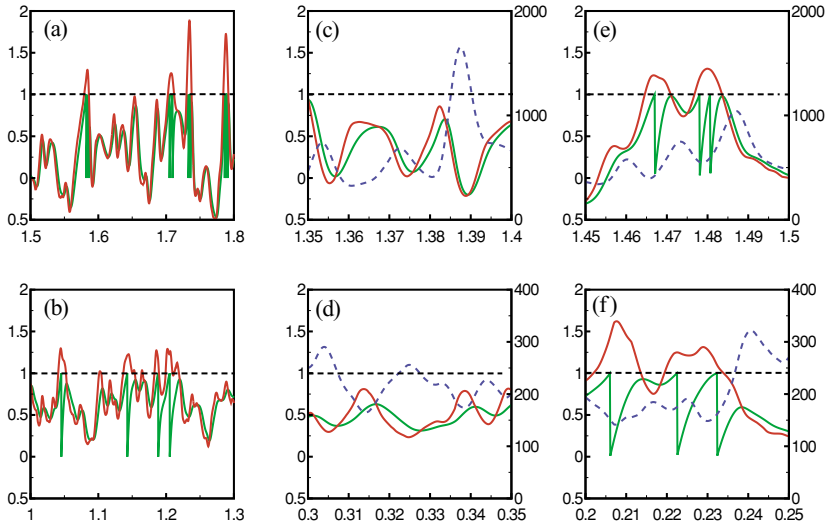

Figure 2. The membrane potential $v(t)$ (green), calculated from the large-scale simulation of the full network, Eq. (1); and the effective reversal potential $V_S(t)$ (red), calculated from the ratio of intracellular current and conductance as in Eq. (7), for an orientation selective excitatory neuron. The neuron (a) is being stimulated by randomly flashed gratings (at optimal spatial and temporal frequency and 100% contrast); and (b) without stimulation. The temporal scale is enlarged in (c)–(f), with the neuron subthreshold in (c) and (d), with (c) and without (d) stimulation; while in (e) and (f) the neuron is suprathreshold (and spiking), with (e) and without (f) stimulation. In (c)–(f) the total conductance is shown as dashed blue, with scale in inverse seconds indicated on the right axis. Intracellular potentials have been normalized to set the threshold to firing at unity (the dashed horizontal line) and reset potential to zero.

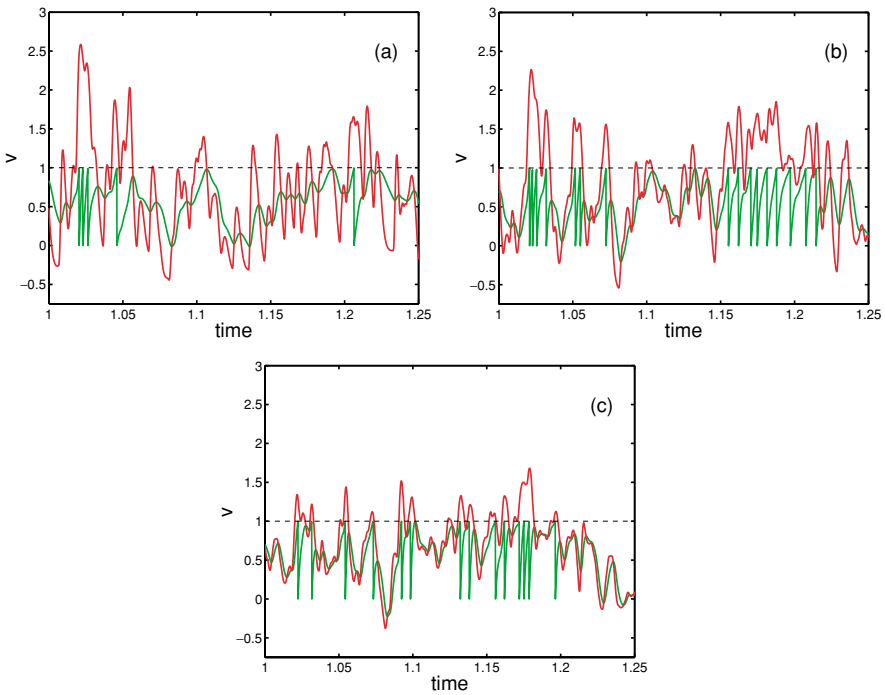

Figure 3. The membrane potential $v(t)$ (green) of a single model neuron impinged upon presynaptically by inhibitory and excitatory spike trains (with Poisson distributed spike-times), and the effective reversal potential $V_S(t)$ (red). Here the Poisson rates are chosen so that $\langle g_T \rangle = 125\ \mathrm{s}^{-1}$ (a), $250\ \mathrm{s}^{-1}$ (b), and $500\ \mathrm{s}^{-1}$ (c), while simultaneously requiring that $\langle I_D \rangle / \langle g_T \rangle = 0.75$. The horizontal dashed line marks the threshold to firing.

We see that even in background, with the two time-scales τ_g and τ_{syn} in approximate balance and not separated, v still tracks V_S rather well. To investigate whether this balance might constitute the transition to high conductance behavior, we consider the dynamics of a single model neuron that is impinged upon presynaptically by excitatory and inhibitory spike trains (here, spike times are Poisson processes). The synaptic strengths are fixed, and the presynaptic spike rates are adjusted to achieve a given mean total conductance $\langle g_T \rangle = \tau_g^{-1}$ (here $\langle \cdot \rangle$ denotes temporal mean), while keeping $\langle I_D \rangle / \langle g_T \rangle$ fixed at 0.75 (below threshold). As in Fig. 2, Fig. 3 shows a detail from the dynamics of v and V_S in response to these spike trains, where respectively, $\tau_g = 2 \cdot \tau_{syn}$ (Fig. 3a), τ_{syn} (Fig. 3b), and $\tau_{syn}/2$ (Fig. 3c). The latter two correspond roughly in conductance time-scales to the model network in background and under stimulation, respectively, while the first is a case where τ_{syn} is the shortest time-scale—a state not captured by our model cortex in its normal operating regime. Figure 3a shows that with a conductance time-scale larger (but not much larger) than that of the synaptic fluctuations, $\tau_g = 8$ ms versus $\tau_{syn} = 4$ ms, the cell's response is an integrator over V_S, not a tracker of its fluctuations, as it is for the $\tau_g = 4$ ms and $\tau_g = 2$ ms cases.

Spiking in a High Conductance State

High conductance asymptotics also allow us to develop simple analytical expressions for the spike rate of a cell in terms of the synaptic inputs. When the effective reversal potential $V_S(t)$ crosses the spiking threshold (a necessary condition for spiking), the slaving of the intracellular potential v to V_S means that $v(t)$ is usually also dragged across threshold to spike. Upon reset to zero, the large conductance again plays an important role by causing $v(t)$ to relax rapidly back towards $V_S(t)$ on the short membrane time-scale, τ_g. If $V_S(t)$ lies yet above threshold, then v will cross threshold again to produce another spike. Using Eq. (9), we can estimate this time to recover from reset to spike threshold, or equivalently, estimate the interspike interval τ_{ISI}. First, let $u_{in} = u_s$ in Eq. (9), where u_s is the first spike time, and set $v(u = u_{in}) = 0$ (reset after a spike). We seek the next spike time $u_s^+ = u_s + \Delta u$, where $\Delta u = O(\epsilon)$. Over this short interval, V_S is only slowly varying and can be considered frozen. Evaluating Eq. (9) at $u = u_s^+$, for which $v(u_s^+) = 1$, we find to leading order

$$\Delta u = -\epsilon \log\left(1 - V_S^{-1}\right), \quad V_S > 1,$$

or, returning to dimensional time, and using that g_T also varies slowly over the interspike interval,

$$\tau_{ISI} \simeq -\frac{\log\left(1 - V_S^{-1}\right)}{g_T}, \quad V_S > 1. \tag{13}$$

We see that when $V_S(t)$ is above the spiking threshold, and $v(t)$ is spiking, it is the total conductance g_T that sets the scale for the interspike interval size. When the conductance is doubled, τ_{ISI} is halved—as is demonstrated in Figs. 2e and f.

Equation (13) can then be used to estimate the spiking rate, $M(T; \Delta)$, of a cell during the time interval $(T, T + \Delta)$ as:

$$\frac{\text{No. of Spikes in time } \Delta}{\Delta} \simeq \frac{1}{\Delta} \int_T^{T+\Delta} \left. \frac{-g_T(t)}{\log\left(1 - V_S^{-1}(t)\right)} \right|_{V_S > 1} dt, \tag{14}$$

That is, given the synaptic inputs to a cell, the evaluation of an integral over the suprathreshold time course of V_S estimates the spike rate of that cell.

Others have invoked a separation of time-scales, such as "slow" synapses, to convert conductance based models of spiking neurons to rate models (e.g. Ermentrout, 1994; Bressloff and Coombes, 2000). Here we have invoked a similar separation of time-scales, but based instead on the observation of large, primarily inhibitory, conductances in our model cortex when under stimulation.

To illustrate the utility and accuracy of Eq. (14) in predicting spike rates, consider Fig. 4, which shows V_S and g_T for a neuron near an orientation pinwheel center, being stimulated by an 8 Hz, full contrast drifting grating (set at preferred orientation). V_S and g_T are shown (the dashed curves) for 10 successive cycles of the stimulus. Also shown are their cycle averages $\bar{V}_S$ and $\bar{g}_T$ (solid curves, computed from 72 cycles). Clearly, both V_S and g_T have substantial fluctuations relative to their cycle averages, and these fluctuations will also have a substantial effect on the average modulation and onset of firing. For example, the cycle average $\bar{V}_S$ being at spiking threshold will not predict the onset of cell firing, as the fluctuations of V_S above threshold can persist even when $\bar{V}_S$ is well below. It is these fluctuations that are resolved in the high conductance state, and their contributions captured by Eq. (14).

Figure 5a compares the cycle averaged spike rate, $\bar{M}$, over the course of the stimulus cycle, found by counting spikes in the cortical network simulation (points), with

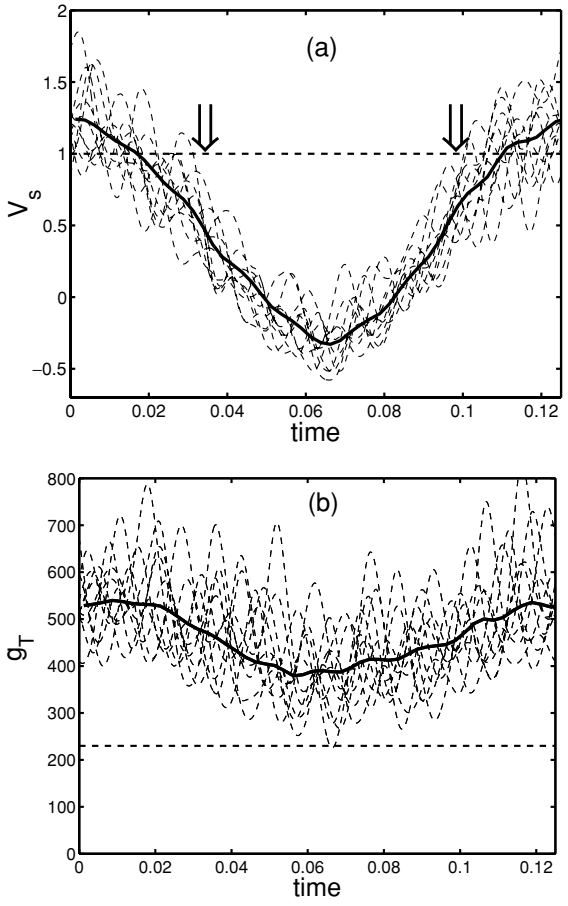

Figure 4. **a:** The dynamics of the effective reversal potential V_S for a neuron of the cortical network model. This neuron is near an orientation pinwheel center, and the network is being stimulated by an 8 Hz, full contrast drifting grating, set at the preferred orientation of the neuron. The dashed curves are V_S for 10 successive cycles of the stimulus. The solid curve is the cycle average of V_S, computed from 72 stimulus cycles. The horizontal dashed line marks the threshold to firing, and the arrows mark the times of offset and onset of firing during the stimulus cycle, as seen in Fig. 5a. **b:** The corresponding dynamics of the total conductance g_T. The horizontal dashed line marks the mean conductance level in the absence of visual stimulation (230 s^{-1}).

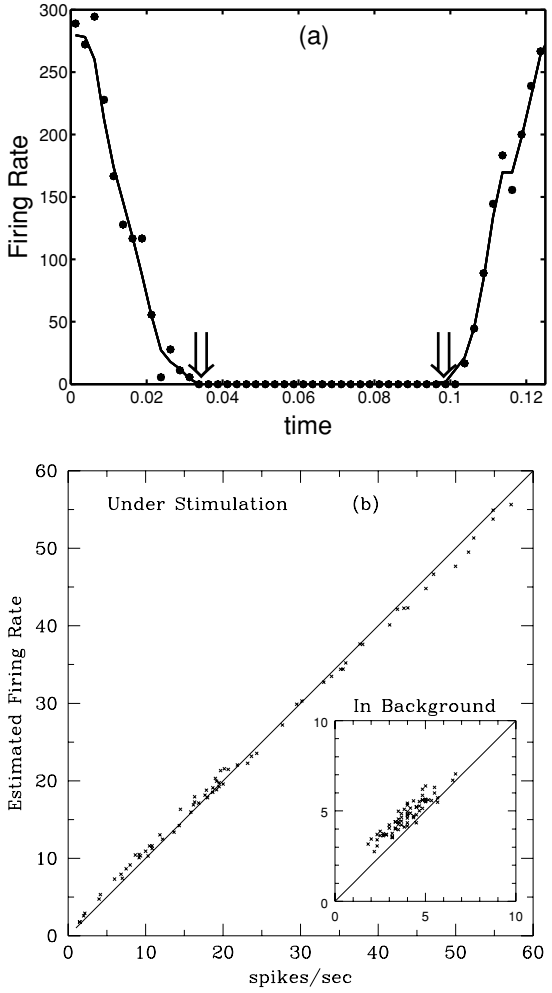

Figure 5. **a:** Comparison of firing rates calculated from spiking in the large-scale simulation with asymptotic estimates. Panel (a) shows cycle-averaged firing rates for the neuron of Fig. 4. The points are calculated by counting spikes in the large-scale simulation of the full network, Eq. (1). The solid curve is calculated using the asymptotic formula Eq. (14). All cycle averages are found from 72 cycles of the stimulus. The arrows mark the times of offset and onset of firing during the stimulus cycle; cf. Fig. 4a. While the agreement shown here is typical, this model neuron is among those with the highest firing rates in our simulations. **b:** Panel (b) shows a further comparison of asymptotic estimates of firing rates with results from simulation: A "scatter plot", over a subpopulation of 70 neurons, of the time-averaged firing rates measured in the large-scale simulations, against those predicted by Eq. (14). The inset shows these results for the same set of neurons, but now in the absence of visual stimulation.

the estimate to $\bar{M}$ given by Eq. (14) (solid curve). For the former, the spike count was binned into 50 subintervals of the stimulus period (of size $\Delta = 0.125/50$), with the cycle average taken over 72 cycles of the stimulus. In the same way, the integral in Eq. (14) was found by numerical quadrature over each subinterval of the stimulus cycle (again of size Δ, with $\Delta \gg \delta t$, the temporal resolution of the simulation), and also cycle averaged over the 72 cycles of the stimulus. The agreement is very good, with Eq. (14) capturing the magnitude, onset, and time-course of firing over the stimulus cycle. Further, for a group of 70 neurons from the simulation, Fig. 5b shows a "scatter plot" comparing firing rates over the stimulus period as predicted

by Eq. (14), against those measured by counting spikes in the full network simulations. Again, the agreement between the full simulations and the asymptotic estimates is very good. In the inset is shown this same comparison, but in the absence of visual stimulation. In this case, the total conductance is lowered, leaving τ_g and τ_{syn} in near balance, and ϵ thus larger than when under visual stimulation. While Eq. (14) still does a reasonable job in predicting firing rates, we expect, and observe, a general deterioration in its accuracy. (As yet another point of comparison, for the sample simulations shown in Fig. 3, the error in calculating spike rates using the asymptotic formula, Eq. (14), is 24%, 10%, and 3% for $\tau_g = 8$, 4, and 2 ms, respectively.)

Hence, as with the slaving of the intracellular potential v to subthreshold V_S, we find that the firing of cells in our model cortical network is well described by our high conductance asymptotic analysis.

It is clear from Figs. 4a and 5a that there is a strong correlation between the long temporal scale modulation of the effective reversal potential V_S (on the τ_{lgn} time-scale) and the modulation in the firing rate. We consider this relation in Fig. 6 by plotting the cycle averaged firing rate $\bar{M}$ (and its estimate) from Fig. 5a, against the cycle averaged potential $\bar{V}_S$. (During the the stimulus cycle, the firing rate both rises and falls, transiting through nearly equal values of $\bar{V}_S$. This gives the two, nearly overlying curves—one for rising, one for falling—seen in the figure.) This relation shows a monotonic increase in firing rate with increase in potential $\bar{V}_S$, with the onset of firing occurring well below the threshold to firing (i.e. at $V > 1$) of the intracellular potential v in the I&F dynamics. This spanning of the firing threshold illustrates how fluctuations in the synaptic inputs contribute to creating a network response, even when the mean potential lies below threshold.

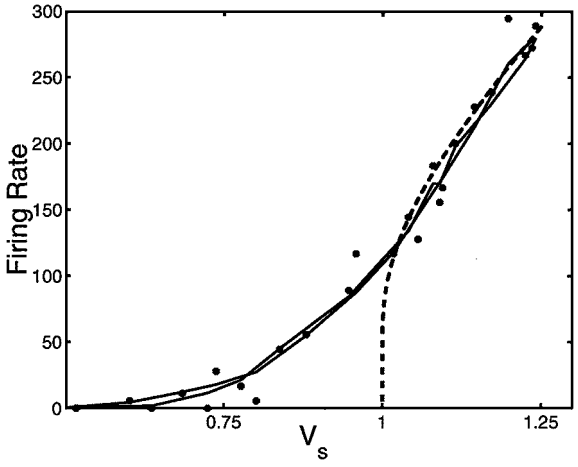

Figure 6. The cycle averaged firing rates (points and solid curves, as in Fig. 5) plotted against the cycle averaged effective reversal potential $\bar{V}_S$. During the stimulus cycle, the firing rate rises and falls, and in so doing transits through nearly equal values of $\bar{V}_S$. This gives the two, nearly overlying curves, and sets of data points, seen in the figure. The dashed curve shows the simplified estimate of firing rate versus $\bar{V}_S$ given in Eq. (15). Note that this estimate obtains only for $\bar{V}_S > 1$.

While the total conductance g_T is also modulated, and in register with V_S, it is much less so. This is because g_T is dominated by its inhibitory component, which, as predicted by our cortical model, is unmodulated for a drifting grating stimulus (Wielaard et al., 2001). Still, the overall scale of the firing rate is set by the total conductance. This is illustrated by the dashed curve in Fig. 6, which shows the simple firing rate estimate

$$\text{Firing Rate} \sim -\frac{\langle \bar{g}_T \rangle}{\log\left(1 - \bar{V}_S^{-1}\right)}, \quad \text{for } \bar{V}_S > 1, \quad (15)$$

where $\langle \bar{g}_T \rangle$ is simply the mean of the relatively unmodulated g_T. This estimate does capture the magnitude and rise of firing at high rates, though not the overall curvature of the data, or its spanning the threshold to firing, both arising from the substantial fluctuations relative to average behavior (Fig. 4a and b).

In the Absence of Visual Stimulation

While the total conductance in the absence of visual stimulation ($\simeq$230 s^{-1}; see Table 2) is significantly higher than the leakage conductance of a single cell (50 s^{-1}), it is not high enough to produce a clear separation from the time-scale of synaptic interactions. In fact, the membrane time-scale $g_T^{-1} \simeq 4$ ms is comparable to the synaptic time-scale τ_{syn}. Yet comparisons with numerical experiments show that predictions of the I/O relationships remain surprisingly accurate, even in the absence of visual stimulation: Fig. 2b shows that the subthreshold membrane potential $v(t)$ remains close to $V_S(t)$, while Fig. 2f (when compared with Fig. 2e) shows that the time for relaxation after firing a spike continues to scale by g_T^{-1}. The inset in the scatter plot of Fig. 5b shows that I/O formula (14) retains good order of magnitude accuracy. This suggests that the I/O relations can be used for rough estimates, even in the absence of visual stimulation where there is no clear separation of time-scales.

The distribution of interspike intervals (the ISI distribution) has been measured for Simple cells in layer $4C\alpha$ in the absence of stimulation (Mechler, 1997), and found to peak around 10 ms. Thus, the numerical model's predicted 8 ms peak in its ISI distribution is in quite good agreement with biological observation. Moreover, we note that the large background conductances we observe lie within the range postulated by Bernander et al. (1991).

Components of the Conductances

In addition to high conductance, the parameter regime at which the computational cortex operates is one of near balance of excitatory and inhibitory currents,

$$g_E V_E \simeq g_I |V_I|.$$

This balance, together with the relative sizes of the two reversal potentials ($V_E \gg |V_I|$), implies large inhibitory conductances ($g_I \simeq |V_E/V_I| g_E > g_E$). The dominance of inhibitory conductances in our large-scale model is seen in Figs. 7 and 8, and in the summary of Table 1.

The total conductance g_T arises from several sources: the LGN, excitatory and inhibitory cortico-cortical activity, and from noise. Figure 7a shows the individual excitatory components—from LGN (blue), other excitatory cortical cells (red), and noise (green)—that make up g_T for the neuron of Fig. 1a and b (under drifting grating stimulation), while Fig. 7b shows the two constituent inhibitory conductances—from inhibitory cortical cells (red), and noise (green). Note that cortico-cortical inhibition dominates all of the component conductances.

Figure 8 shows the component conductances for the neuron of Fig. 1c, experiencing randomly flashed grating stimuli. Again, the inhibitory cortico-cortical contribution dominates.

Table 1. The five components of the total conductance, without visual stimulation, and with drifting grating and randomly flashed grating stimuli. The numbers listed are the approximate minimum and maximum values.

Conductances ($\sec^{-1}$)	Background	Drifting grating	Randomly flashed
LGN	35–35	0–160	0–170
$4C\alpha$, Ex.	0–15	0–65	0–225
Noise, Ex.	0–25	0–25	0–25
$4C\alpha$, In.	20–130	180–600	65–1700
Noise, In.	5–180	5–180	10–200

Table 2. The temporal mean of the total conductance, and the standard deviation of its temporal fluctuations, for one typical neuron near a pinwheel center, and a second typical neuron far from any pinwheel center.

Total cond. ($\sec^{-1}$)	Background	Drifting pref	Drifting orth	Randomly flashed
Near	230 ± 40	475 ± 90	460 ± 70	480 ± 175
Far	230 ± 40	550 ± 100	400 ± 80	480 ± 175

We quantify the conductance sizes further in Tables 1 and 2, which list the maximum and minimum values of the five components of the conductance for the different stimuli: (i) unstimulated, (ii) drifting grating at preferred orientation, and (iii) randomly flashed gratings—as well as the means and standard deviations of the total conductances. The predominance of inhibition allows us to simplify Eq. (7), which defines V_S, and hence also simplify the (subthreshold) slaving relation Eq. (10):

$$\begin{aligned} v(t) \simeq V_S &= \frac{g_E V_E + g_I V_I}{g_L + g_E + g_I} \\ &\simeq \frac{g_E V_E + g_I V_I}{g_I} = V_I \left(1 + K \cdot \frac{g_E}{g_I} \right), \end{aligned} \quad (16)$$

with $K = V_E/V_I$. And so, the modulation of V_S (and hence v) is approximately the ratio of excitatory to inhibitory conductances.

Spatial Distribution of Conductances

As with orientation selectivity (McLaughlin et al., 2000), the value of total conductance for a model neuron also depends on its location within the cortical layer, relative to pinwheel centers. Figure 1a–c showed the total conductance $g_T(t)$ for a typical orientation selective neuron far from a pinwheel center. While such plots for a neuron near a pinwheel center are similar in appearance, there can be interesting differences in magnitude. For example, for drifting grating stimuli, the modulation of the total conductance (between its large value for stimulation at preferred orientation and its smaller response at stimulation orthogonal-to-preferred) is greater for far neurons than near neurons. Indeed, at *preferred orientation*—

$$g_{T,Near} = 475 \pm 90 \text{ s}^{-1}, \quad g_{T,Far} = 550 \pm 100 \text{ s}^{-1};$$

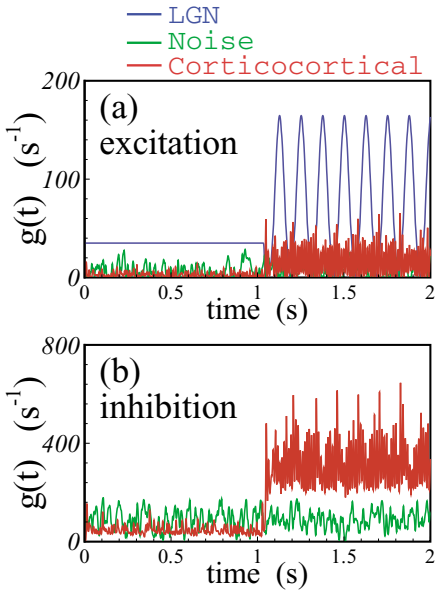

Figure 7. The five components of the total conductance for the neuron in Fig. 1—without visual stimulation and for a drifting grating stimulus (at 8 Hz, switched on after one second). **a:** Excitatory: LGN (blue), cortical interaction from layer 4$C\alpha$ (red) and noise (green). **b:** Inhibitory: cortical interaction from layer 4$C\alpha$ (red) and noise (green). Notice the difference in the vertical scales for (a) and (b).

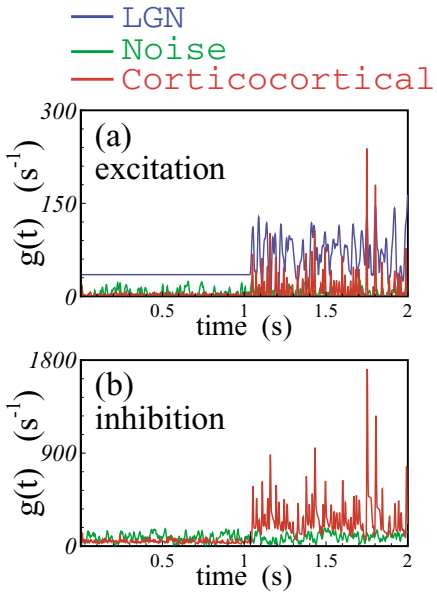

Figure 8. The five components of the total conductance for the neuron in Fig. 1—without visual stimulation and for randomly flashed stimuli (switched on after one second). **a:** Excitatory: LGN (blue), cortical interaction from layer 4$C\alpha$ (red) and noise (green). **b:** Inhibitory: cortical interaction from layer 4$C\alpha$ (red) and noise (green). Notice the difference in the vertical scales for (a) and (b).

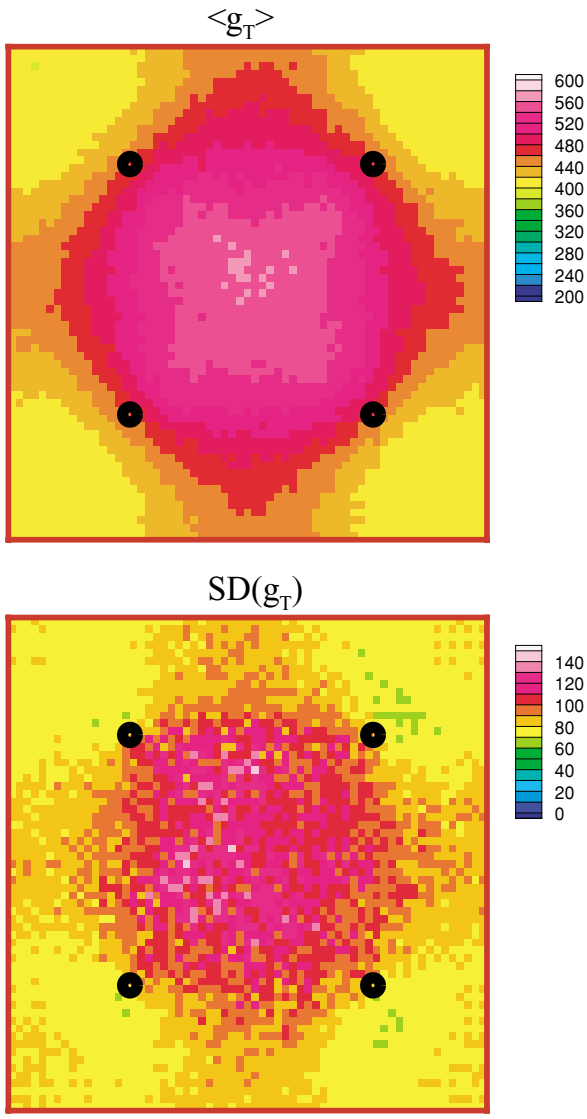

Figure 9. The spatial distribution of the neurons' local patch of the input layer: Upper: temporal averages; Lower: standard deviations of the temporal fluctuations. The black circles show the locations of the 4 pinwheel centers in the model's orientation map.

and at *orthogonal-to-preferred*—

$$g_{T,Near} = 460 \pm 70\ \mathrm{s}^{-1}, \quad g_{T,Far} = 400 \pm 80\ \mathrm{s}^{-1}.$$

On the other hand, for randomly flashed gratings, there is little difference between the conductances and their fluctuations for near and far neurons.

One advantage of large-scale models is the ability to examine the spatial distribution of the properties of

model neurons across the network, and to study these relations with respect to the model's architecture. For drifting grating stimuli, the spatial distribution of the temporal average of the conductances across the local patch of model input layer is shown in Fig. 9a, with the spatial distribution of standard deviation of the temporal fluctuations shown in Fig. 9b. The center region of highest conductance (in violet) overlays those orientation columns best stimulated by the visual stimulus. Further, the average conductance varies smoothly in regions far from the pinwheel centers (labeled by black circles), and even those regions not optimally stimulated (i.e., orientation columns at orthogonal-to-preferred, overlaid by yellow) have conductances well above background values (400 s^{-1}, as compared with background values of 230 s^{-1}). Near the pinwheel centers, the average conductance changes more rapidly in space, over distances of 100 microns, a scale set by the axonal arbors of inhibitory neurons. The fluctuations (Fig. 9b) are significantly larger far from pinwheels than near.

Other stimuli, such as randomly flashed gratings, create very different and distinct conductance maps on the model cortex. In contrast to drifting gratings, the temporal mean and standard deviation of the temporal fluctuations of the conductance for randomly flashed grating stimuli are distributed with relative uniformity across the entire layer (not shown). The population histograms of Fig. 10 confirm these features quantitatively. For instance, for drifting gratings, the conductances depend sensitively upon location within the cortical layer relative to pinwheel centers. Figure 10 shows histograms of all neurons within a disc of radius 100 microns, centered near (Fig. 10a, b, e and f), or far (Fig. 10c, d, g and h), from pinwheel centers. Both the mean of the conductance, and the standard deviation of its temporal fluctuations, are shown. All of the distributions in Fig. 10 are rather tight—except for those of stimulation by a drifting grating (Fig. 10a and b) near a pinwheel center, where the model neurons have broad distributions of both mean conductance and standard deviation. Furthermore, the histograms in Fig. 10b, d, f and h for the standard deviation show that the fluctuations are significantly and uniformly higher for randomly flashed stimuli (Fig. 10f and h) than for drifting gratings (Fig. 10b and d).

Such considerations emphasize that neurons within our computational model tend to behave very differently, whether they are near or far from pinwheel centers. As emphasized in McLaughlin et al. (2000), these distinctions can be traced to a transfer of the "circle of influence upon a given neuron"—from spatial interaction lengths within the cortical layer to interaction lengths in terms of the angle of orientation preference. Because of the spatial extent of the cortico-cortical interactions, and their relationship to the tiling of the cortex by pinwheel patterns of orientation

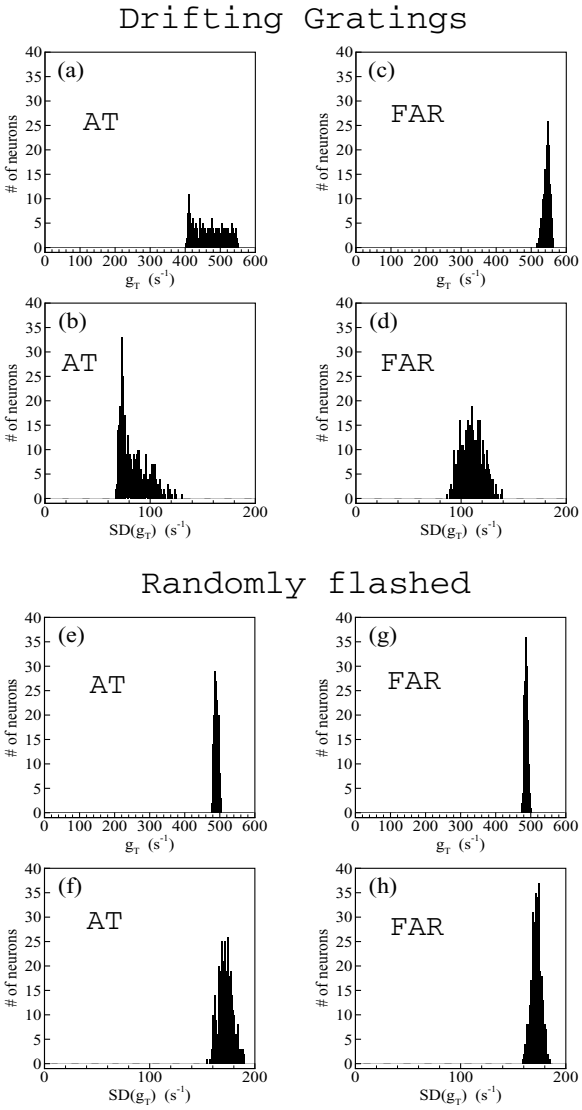

Figure 10. Histograms of the temporal average of the conductance $g_T(t)$ and the standard deviations of its temporal fluctuations, for all neurons within a disc of radius 100 microns, centered AT (Panels a, b, e, f), or far (Panels c, d, g, h), from pinwheel centers. Drifting gratings were used to generate the data in 8a–d, while randomly flashed gratings were used in Panels e–h.

preference, neurons near (or at) a pinwheel center experience cortico-cortical inhibition which is effectively *global in orientation preference*—in contrast to those far from pinwheel centers which experience only cortico-cortical inhibition which is *local in orientation preference*, where these far neurons interact monosynaptically only with neurons of similar orientation preference. This distinction quickly leads to theoretical predictions such as, for drifting gratings,

$$g_{T,Pref,Near} < g_{T,Pref,Far}$$
$$g_{T,Orth,Near} > g_{T,Orth,Far},$$

which are consistent with the numerical results of the computational model (Table 2).

Discussion

Our computational cortex operates in a high-conductance state—a state caused by cortical activity. We emphasize that this high conductance state is not an individual cellular property, and that we are not free to place the network arbitrarily into a high-conductance regime. Rather, in our model the total conductance g_T must be large in order to obtain (i) orientation selectivity in agreement with experiment and (ii) the linearity of Simple cells also observed in experiment. Background activity increases the conductance by a factor of 4–5 when compared with leakage times derived from cells in cortical slices, and high contrast visual stimulation further increases it by another factor of 2. Together, this combined cortical activity increases the total conductance in model neurons by factors of 8–10 over base leakage conductances. This high-conductance state is consistent with recent intracellular measurements of conductances (Borg-Graham et al., 1998; Hirsch et al., 1998; Anderson et al., 2000), as well as with theoretical interpretations (e.g., Bernander et al., 1991). In summary, observational data, simulations, and theoretical interpretations all suggest a high-conductance state as the cortical operating point when under visual stimulation.

If the membrane conductance is high enough, it is intuitively clear that the membrane potential will be slaved to an effective reversal potential, and will relax back rapidly if displaced away from it. This will occur if the membrane time-scale $\tau_g = [g_T]^{-1} \ll \tau_{syn}$, the synaptic time-scale, i.e. τ_g and τ_{syn} are *well separated*. Asymptotic methods then produce I/O relations which establish the slaving of the membrane potential to the effective reversal potential, and identify other detailed properties such as the temporal phase lag by which the membrane potential trails the effective reversal potential. These I/O relations further describe the firing rate of a neuron directly in terms of the dynamics of its total conductance and effective reversal potential.

However, in our model the conductance time-scale $\tau_g \simeq 2$ ms is only a factor of two smaller than the synaptic time-scale, $\tau_{syn} = 4$ ms. Nonetheless, we find that this moderate separation of time-scales is sufficient to allow the cell's dynamics to be described very accurately in terms of the asymptotic analysis.

Possible Functions of High Conductance

Neurons within a less active network respond by smoothing over synaptic time-scales, rather than closely tracking their associated fluctuations (see Fig. 3). This difference has possible functional consequences: the performance of individual neurons as coincidence detectors, burst generators, and pattern transmitters could improve with increasing network activity. Also, at each stage of cortical processing, whereas τ_{syn} limits the time-scale of the input, τ_g can replace τ_{syn} as the limiting time-scale of the output. Related ideas have been discussed in the literature. (See the reviews of Koch et al., 1996; Usrey and Reid, 1999, and references therein; see also Tsodyks and Sejnowski, 1995; van Vreeswijk and Sompolinsky, 1996 for discussions of time-scales associated with balanced network states and chaotic fluctuations.) Another possible function of a high conductance state in a network dominated by inhibition, as we have studied here, is that it allows the network response to follow the ratio of excitatory to inhibitory conductances in a smoothly graded and monotonic fashion.

Coincidence Detection

Neurons responding at high conductance can act as coincidence detectors, with the temporal resolution determined by the cortical synaptic time-scales τ_{syn} inherent in the total conductance g_T and the difference current I_D (recall Eq. (6)): Let G_E denote the time-course of conductance changes in response to a spike arriving from an excitatory neuron. Consider then two incident excitatory spikes, arriving at times $t_1 < t_2$, with separation $\Delta = t_2 - t_1$. In the high conductance regime, the consequent postsynaptic response over the baseline I_D

and g_T is given by

$$v(t) \approx \frac{I_D + V_E(G_E(t-t_1) + G_E(t-t_2))}{g_T + G_E(t-t_1) + G_E(t-t_2)}.$$

Here, the peak increase in potential $v(t)$ above baseline increases monotonically as the spike separation Δ decreases. Thus, two spikes arriving closely in time could act together and cause $v(t)$ to cross threshold and produce a postsynaptic spike (or spikes). For a larger time separation Δ (exceeding the synaptic timescale of $G_E(t)$), the two would act independently, and if neither individually produced voltage changes of sufficient size to cross threshold, the postsynaptic neuron would not fire. It follows that neurons in a high conductance regime, with $\tau_g \ll \tau_{syn}$, could act as coincidence detectors with a temporal resolution of τ_{syn}. This conclusion is supported by recent measurements (Roy and Alloway, 2000) on cat somatosensory cortex, which find that thalamo-cortical spikes separated in time by less than 6–8 ms enhance cortical response, while little enhancement is found when the temporal separation of the incoming spikes exceeds 6–8 ms.

Burst Generation

Next, consider a cortical neuron within a high-conductance state acting as a "burst generator": Assume that, because of incident spikes, its effective reversal potential crosses the firing threshold from below at time t_1, and remains above threshold until time $t_2 = t_1 + \Delta$. If g_T is sufficiently large, the neuron will fire a sequence of spikes in time interval $t_2 - t_1 = \Delta$, where Eq. (14) estimates the number of spikes (N) fired by the neuron in the sequence as

$$N \propto \frac{\Delta}{\tau_g} = \Delta \cdot g_T$$

(i.e. the interspike times within the sequence scale as $O(\tau_g = g_T^{-1})$). When synaptic input from other neurons comes in bursts, they could cause a postsynaptic neuron to likewise fire a burst of spikes, and therefore through this mechanism the cortical neuron acts as a "burst transmitter".

Thus, I/O analysis identifies two distinct time-scales for an high-conductance neuron when acting as a coincidence detector or as a burst transmitter. For detecting coincidence in the arrival of two spikes, the temporal resolution of the input is set by τ_{syn}, the synaptic timescale. Within an outgoing sequence of spikes, the conductance size itself sets the interspike intervals as g_T^{-1}.

The Firing Rate Closely Follows the Conductances

Our network produces the nearly linear responses of Simple cells, whose computations are believed to be crucial for many tasks of visual perception (see Wielaard et al. (2001) and the references therein). This is accomplished through a nonlinear network whose conductance is high, and dominated by inhibition. In this high conductance state, Eq. (16) indicates that $V_S \simeq V_I(1 + K \cdot (g_E/g_I))$, or that the modulation of the effective reversal potential of a neuron will be approximately proportional to its ratio of excitatory to inhibitory conductances. This is important because in our Simple cell network, the excitatory conductance g_E is dominated by, and so follows closely, its geniculate component. Following our understanding, and instantiation, of the cortical architecture (see McLaughlin et al., 2000; Wielaard et al., 2001), the inhibitory conductance, that divides g_E, is only cortico-cortical, being a sum over the activity of many nearby inhibitory neurons. Thus in V_S we see the geniculate input conductance being normalized by a population response. Figure 6 shows, for this case of steady-state tuning, that the firing rate is a smoothly increasing function of V_S. The overall scale of firing, or the gain, is set by the total conductance, which in our model is dominated by cortico-cortical inhibition.

This may be the most profound of the given, possible functions of the cortex operating in high conductance: The firing rate is the result of an accurate and smoothly graded computation of the ratio of excitatory to inhibitory conductances. This may be a necessary task that underlies the computations of Simple cells.

Acknowledgment

The authors acknowledge the support of the Sloan Foundation for the New York University Theoretical Neuroscience Program, National Institutes of Health Grant 2R01-EY01472, and National Science Foundation Grants DMS-9971813 and DMS-9707494. The authors thank Louis Tao for useful conversations and technical assistance.

References

Anderson JS, Carandini M, Ferster D (2000) Orientation tuning of input conductance, excitation, and inhibition in cat primary visual cortex. J. Neurophysiol. 84: 909–926.

Azouz R, Gray CM, Nowak LG, McCormick DA (1997) Physiological properties of inhibitory interneurons in cat striate cortex. Cereb Cortex 7: 534–545.

Bernander O, Douglas R, Martin K, Koch C (1991) Synaptic background activity influences spatiotemporal integration in single phyrmidal cells. Proc. Nat. Acad. Sci. USA 88: 11569–11573.

Benardete E, Kaplan E (1999) The dynamics of primate M retinal ganglion cells. Vis. Neurosci. 16: 355–368.

Borg-Graham L, Monier C, Fregnac Y (1998) Visual input evokes transient and strong shunting inhibition in visual cortical neurons. Nature 393: 369–373.

Bressloff P, Coombes S (2000) Dynamics of strongly coupled spiking neurons. Neural Computation 12: 91–129.

Callaway E (1998) Prenatal development of layer specific local circuits in primary visual cortex of the macaque monkey. J. Neurosci. 18: 1505–1527.

Callaway E, Wiser A (1996) Contributions of individual layer 2 to 5 spiny neurons to local circuits in macaque primary visual cortex. Visual Neuroscience 13: 907–922.

De Valois R, Albrecht D, Thorell L (1982) Spatial frequency selectivity of cells in macaque visual cortex. Vision Res. 22: 545–559.

Ermentrout GB (1994) Reduction of conductance based models with slow synapses to neural networks. Neural Computation 6: 679–695.

Gibson J, Beierlein M, Connors B (1999) Two networks of electrically coupled inhibitory neurons in neocortex. Nature 402: 75–79.

Hirsch J, Alonso JM, Reid R, Martinez L (1998) Synaptic integration in striate cortical simple cells. J. Neuroscience 15: 9517–9528.

Koch C (1999) Biophysics of Computation. Oxford University Press, Oxford.

Koch C, Rapp M, Segev I (1996) A brief history of time constants. Cerebral Cortex 6: 93–101.

Lund J (1987) Local circuit neurons of macaque monkey striate cortex neurons of laminae 4C and 5A. Journal of Comparative Neurology 257: 60–92.

Lund J, Wu C (1997) Local circuit neurons of macaque monkey striate cortex neurons of laminae 1 and 3A. Journal of Comparative Neurology 384: 109–126.

Lund J, Yoshioka T (1991) Local circuit neurons of macaque monkey striate cortex neurons of laminae 4B 4A and 3B. Journal of Comparative Neurology 311: 234–258.

McLaughlin D, Shapley R, Shelley M, Wielaard J (2000) A neuronal network model of macaque primary visual cortex (v1): Orientation selectivity and dynamics in the input layer $4C\alpha$. Proc. Natl. Acad. Sci. USA 97: 8087–8092.

Mechler F (1997) Neuronal response variability in the primary visual cortex. Ph.D. diss., New York University.

Ringach D, Hawken M, Shapley R (1997) Dynamics of orientation tuning in macaque primary visual cortex. Nature 387: 281–284.

Roy S, Alloway K (2000) Coincidence detection or temporal integration? What the neurons in somatosensory cortex are doing. Journal of Neuroscience 21: 2462–2473.

Tsodyks M, Sejnowski T (1995) Rapid state switching in balanced cortical network models. Network 6: 111–124.

Usrey WM, Clay Reid R (1999) Synchronous activity in the visual system. Annu. Rev. Physiol. 61: 435–456.

van Vreeswijk C, Sompolinsky H (1996) Chaos in neuronal networks with balanced excitatory and inhibitory activity. Science 274: 1724–1726.

Wielaard J, Shelley M, Shapley R, McLaughlin D (2001) How simple cells are made in a nonlinear network model of the visual cortex. J. Neuroscience 21: 5203–5211.

Wiser A, Callaway E (1996) Contribution of individual layer 6 pyramidal neurons to local circuitry in macaque primary visual cortex. Journal of Neuroscience 16: 2724–2739.